# Efficient nanostructured materials to reduce nutrient leaching to overcome environmental contaminations

**Farwa Nadeem**
University of Agriculture
**Muhammad Asif Hanif**
drmuhammadasifhanif@gmail.com
University of Agriculture
**Najla AlMasoud**
Princess Nourah bint Abdulrahman University
**Taghrid S. Alomar**
Princess Nourah bint Abdulrahman University
**Adnan Younis**
University of Agriculture

**Article**

**Keywords:** 28-homobrassinolide, ethephon, menthol, Mentha arvensis L. LIBS, DSC-TGA, SEM

**Posted Date:** October 6th, 2023

**DOI:** https://doi.org/10.21203/rs.3.rs-3361313/v1



**Additional Declarations:** No competing interests reported.

**Version of Record:** A version of this preprint was published at Scientific Reports on February 27th, 2024.
See the published version at https://doi.org/10.1038/s41598-024-54049-1.

# Abstract

Nutrient leaching is a major reason for fresh and ground water contamination. Menthol is the major bioactive ingredient of *Mentha arvensis* L. and one of the most traded products of the global essential oil market. The indigenous production of menthol crystals in the developing countries of the world can prove to be the backbone for the local growers and poor farmers. Therefore, present research was designed to check the effects of nanostructured plant growth regulators (PGRs) (28-homobrassinolide and ethephon) with reduced leaching potentials on the essential oil and menthol (%) of *Mentha arvensis* L. The prepared nanoformulations were characterized by the Fourier transform infrared (FTIR) spectroscopy, Laser induced breakdown spectroscopy (LIBS), Differential scanning colorimetry-thermal gravimetric analysis (DSC-TGA), Scanning electron microscopy (SEM) and Atomic absorption spectrometry (AAS). The menthol (%) was determined by modified spectrophotometric and gas chromatographic (GC) method. The highest essential oil (%) was obtained by the 28-homobrassinolide-Zn-NPs-L-II (0.92 ± 0.09%) and ethephon-Ca-NPs-L-III (0.91 ± 0.05%) as compared to the control (0.65 ± 0.03%) and blank (0.62 ± 0.09%). The highest menthol (%) was obtained by the 28-homobrassinolide-Ca-NPs-L-I (80.06 ± 0.07%), 28-homobrassinolide-Ca-NPs-L-II (80.48 ± 0.09%) and 28-homobrassinolide-Ca-NPs-L-III (80.84 ± 0.11%) and ethephon-Ca-NPs-L-III (81.53 ± 0.17%) and ethephon-Zn-NPs-L-II (81.93 ± 0.26%) as compared to the control (67.19 ± 0.14%) and blank (63.93 ± 0.17%).


# 1. Introduction

The *Mentha arvensis* L. (menthol mint, wild mild, corn mint, Japanese mint and field mint) is an important aromatic medicinal plant having number of applications in pharmaceutical industries, cosmetic products and food and flavouring agents [1]. The essential oil of *Mentha arvensis* L. contains many bioactive components such as oxygenated monoterpenes, monoterpene hydrocarbons, oxygenated sesquiterpenes, sesquiterpene hydrocarbons, ester, ketone, alcohol and all terpene related compounds [2]. The menthol is the major secondary metabolite of *Mentha arvensis* L. [1], having analgesic and pain relieving effects, with transient receptor potential melastatin-8 (TRPM8) [3]. According to an estimate, the global essential oil market is valued approximately 10.3 billion USD in 2021 and expected to reach upto 16.0 billion USD by the end of 2026, with the CAGR of 9.3% [4]. As per the data of "Observatory of Economic Complexity", menthol ($C_{10}H_{20}O$) is the world's 2015th most traded product with the total imports and exports upto millions of USD. As per the recent report of 2020, currently the global menthol market is around 930 Million USD and expected to reach upto 1298.4 Million USD till the end of 2027, with the CAGR of 4.8% during the forecasted period of 2021 to 2027 [5].

The percentage of menthol in *Mentha arvensis* L. varies by varying the harvesting time, geographical location, availability of water, fertility of soil, climate change, biotic and abiotic stresses and soil texture [6]. Therefore, exogenous application of plant growth regulators (PGRs) (including plant growth promoters and plant growth inhibitors) helps to ensure the additional salt stress, for triggering the biosynthesis of secondary metabolites in plants. The nanostructured plant growth regulators have proved to be the

proficient elicitors for stimulating the production of secondary metabolites, with the minimum agricultural input [7]. These natural or synthetic biostimulants not only controls the total antioxidant compounds of herbaceous plants but also elucidate the physiological responses and biochemical pathways for the proper growth and development. Some of the major types of plant growth regulators include (i) auxins (indole-3-acetic acid (IAA), indole-3-acetonitrile (IAN), indole-3-acetaldehyde (IAc), ethylindole acetate and indole-3-pyruvic acid (IPyA)) (ii) cytokinins (ribosylzeatin, zeatin, iso-pentinyladenine and dihydrozeatin) (iii) gibberellins ($GA_4$, $GA_3$ and $GA_7$) (iv) ethylene releasing compounds (ethephon and ethrel) (v) brassinosteroids (dolicholide, 28-homodolicholide, casta-sterone, dolichosterone, 28-homodolichosterone and typhasterol) (vi) jasmonates ( jasmonic acid) and (vii) strigolactones (strigol, $GR_{24}$ and orobanchol).

The brassinosteroids are naturally occuring steroidal hormones of plants that induce the stress tolerance in aromatic herbs, by regulating the production of reactive oxygen species (ROS) in living cells. The exogenous application of 28-homobrassinolide improves catalytic activities of monodehydroascorbate reductase, superoxide dismutase, dehydroascorbate reductase, ascorbate peroxidase, glutathione reductase and catalases. The 28-homobrassinolide also improves the redox potential of naturally occuring antioxidant compounds of plants to tolerate abiotic stresses [8]. The ethephon belongs to the ethylene releasing compounds that potentially interferes with the growth processes and hormonal systems of plants. Ethephon is a known plant growth retardant (PGR), having growth inhibiting effects. It improves the opening and closing of stomata, induces the sterility of pollens, influences the biosynthesis of secondary metabolites, enhances the herbicidal efficacy, eradicates the pests, and depresses the formation of vesicular arbuscular mycorrhizae. The mode of action of ethephon in plants is quite similar to the mode of action of auxins that involve two step processes including (i) biosynthesis of abscisic acid and (ii) production of ethylene in plants [9,10]. Therefore, present research was designed to check the effects of nanostructured PGRs (28-homobrassinolide and ethephon) on the essential oil contents and menthol percentage of *Mentha arvensis* L.

## 2. Materials and methods

## 2.1. Chemicals and reagents

All the chemicals, reagents and gas chromatographic standards used in this research work were of analytical grade.

## 2.2. Preparation of nanostructured PGRs

### 2.2.1. Ethylene diammine tetraacetic acid based nanoparticles

The 28-homobrassinolide-EDTA-NPs and ethephon-EDTA-NPs were prepared by separately dissolving 90 g of 28-homobrassinolide (pH = 3–4) and ethephon (pH = 2) in 80 mL and 30 mL of distilled water (reaction temperature: 35°C, reaction time: 1 hour and stirring intensity: 700 rpm). After the 1 hour of

continuous stirring, 5.364 g of $Na_2EDTA.2H_2O$ (dissolved in 10 mL of distilled water), was added in the reaction mixtures (reaction temperature: 35°C, reaction time: 1 hour and stirring intensity: 700 rpm). The 28-homobrassinolide formed smooth, creamy and thick off-white paste which changed into thin, off-white and easily stirrable precipitates (pH = 4–5) while ethephon showed no change in physical state except off-white colour changed into pure white grains (pH = 3). After the completion of stirring period, concentrated HCl was added (pH = 2) in the mixtures (reaction temperature: 35°C, reaction time: 4 hours and stirring intensity: 1000 rpm) and let them to stir again. After the 4 hours of stirring, the prepared NPs were allowed to settle, upper liquid layers were decanted, and NPs were dried (at 45°C for about 6 to 8 hours) for further use.

## 2.2.2. Silica based nanoparticles

The 28-homobrassinolide-Si-NPs and ethephon-Si-NPs were prepared by dissolving 90 g 28-homobrassinolide (pH = 4) and ethephon (pH = 2) separately in 130 mL and 140 mL of distilled water (reaction temperature: 35°C, reaction time: 1 hour and stirring intensity: 700 rpm). After the completion of 1 hour, 3.5 g $Na_2O_3Si.9H_2O$ was added in the reaction mixtures (pH = 9) and allowed to stir again (reaction temperature: 35°C, reaction time: 1 hour and stirring intensity: 700 rpm). This stirring period lead to the formation of off-white precipitates of 28-homobrassinolide and converted smooth skin paste of ethephon into brownish gelatinous liquid, having shiny appearance. After the 1 hour of continuous stirring, highly concentrated $H_2SO_4$ was gradually added in a dropwise manner till the pH = 5.5. In case of 28-homobrassinolide, only few drops changed the colour of granular solution into light green, while no change was observed in the physical state of ethephon. At this pH range, the concentrated solution of $CaCl_2$ was added in the mixtures and let them to stir again (reaction temperature: 35°C, reaction time: 12 hours and stirring intensity: 700 rpm). As a result of this stirring, clear solution of 28-homobrassinolide turned into white foamy mixture while clear brown solution of ethephon changed into densely clouded brownish liquid. After 12 hours of stirring, dark brownish liquid was converted into light brown solution. These mixtures were centrifuged at 4000 rpm, upper liquid layers were separated and thick precipitates were dried (at 45°C for about 6 to 8 hours) and finely ground.

## 2.2.3. Calcium based nanoparticles

The 28-homobrassinolide-Ca-NPs and ethephon-Ca-NPs were prepared by dissolving the 90 g of 28-homobrassinolide (pH = 3–4) and ethephon (pH = 2) in 80 mL and 30 mL of distilled water separately (reaction temperature: 35°C, reaction time: 1 hour and stirring intensity: 700 rpm). After the 1 hour of continuous stirring, 850.32 g $Ca(NO_3)_2.4H_2O$ (pH = 5) was added in the reaction mixtures (reaction temperature: 35°C, reaction time: 1 hour and stirring intensity: 700 rpm), resulting in the conversion of pale yellow granular solution of 28-homobrassinolide into smooth off-white paste (pH = 2). However, no change was observed in the physical state of ethephon (pH = 2). After this stirring period, 850.32 g of $Na_2CO_3$ (pH = 10) was added in the above mentioned solutions (reaction temperature: 35°C, reaction time: 1 hour and stirring intensity: 700 rpm), resulting in the formation of yogurt like creamy mixture of 28-homobrassinolide (pH = 6) from smooth off-white paste. However, mixture of ethephon reduced the

reaction temperature and showed a unique property of instant bubbling after the addition of $Na_2CO_3$, due to the release of carbon dioxide and ethylene gas. After the completion of 1 hour, fully concentrated solution of NaOH was added in a dropwise manner, till the pH = 10 and allowed the mixtures to stir again (reaction temperature: 35°C, reaction time: 18 hours and stirring intensity: 700 rpm). In case of ethephon-Ca-NPs, the apparent colour of ethephon changed from champion brown to golden brown and then dark brown to the dark black. After 18 hours of continuous stirring, both the mixtures were centrifuged at 4000 rpm, decanted and dried (at 45°C for about 6 to 8 hours).

## 2.2.4. Zinc based nanoparticles

The 28-homobrassinolide-Zn-NPs and ethephon-Zn-NPs were prepared by dissolving 90 g 28-homobrassinolide (pH = 2) and ethephon (pH = 2) separately in 70 mL and 30 mL distilled water (reaction temperature: 35°C, reaction time: 1 hour and stirring intensity: 700 rpm). After this period of time, 0.104 g $Zn(NO_3)_2.6H_2O$ (pH = 6) was added in the reaction mixtures and let them to stir (reaction temperature: 35°C, reaction time: 1 hour and stirring intensity: 700 rpm). This stirring period led the formation of thick off-white granular solution of 28-homobrassinolide having pH = 3 and converted skin off-white paste of ethephon into easily stirrable quite thin solution (pH = 2). After the 1 hour of stirring period, 0.075 g $Na_2SO_4$ (pH = 8) was added in the solutions and let them to stir again (reaction temperature: 35°C, reaction time: 1 hour and stirring intensity: 700 rpm). The 28-homobrassinolide showed no change in physical state while ethephon showed conversion of smoothly stirring off-white solution into turbid mixture. After the completion of stirring, concentrated NaOH was added in the mixture (reaction temperature: 35°C, reaction time: 15 hours and stirring intensity: 700 rpm), resulting in the formation of light green solution (pH = 8) of 28-homobrassinolide and crystal clear pure golden liquid (pH = 9) of ethephon. After the 15 hours, both these reaction mixtures were allowed to settled, upper liquid layers were decanted, and skin off-white and dark brown precipitates were dried (at 45°C for about 6 to 8 hours) for further use.

# 2.3. Preparation of Hoagland solution

The Hoagland solution was prepared by mixing the macro-nutrients, micro-nutrients and complexing agents as per the calculations mentioned in [11].

# 2.4. Preparation of field and application of doses

The freshly harvested young stems of *Mentha arvensis* L. were collected from the Rosa Project of Institute of Horticultural Sciences, University of Agriculture, Faisalabad, Pakistan. These healthy stems were cut into 5 to 7.5 cm pieces and placed into 8 to 10 cm deep furrow at the approximate distance of 45 cm [12]. The young plants were watered at alternate days for 21 days after plantation, prior to the application of doses [1]. After the growth of young plants, both nanostructured PGRs and fixed concentration nutrient media, were applied to the plants at three different concentrations (low: 25 ppm (Level-I), medium: 100 ppm (Level-II) and high: 250 ppm (Level-III)) for consecutive 20 weeks through root application [13].

## 2.5. Harvesting and extraction of essential oil

After the completion of dose application and growth of *Mentha arvensis* L., the healthy and matured plants were harvested and shade dried, prior to the extraction of essential oil [14]. The essential oil was extracted through Clevenger type hydrodistillation apparatus [15]. The extracted essential oil was collected in separate containers, dried through anhydrous sodium sulphate, filtered with micro-filters and refrigerated for the further analysis. The essential oil (%) was calculated as per the following formula (Eq. 1):

$$\mathrm{Yieldofessentialoil\,(\%)} = \frac{\mathrm{Netweightofessentialoil\,(g)}}{\mathrm{Totalweightofdriedbiomass\,(g)}} \times 100 \ldots\ldots\ldots (\mathrm{Eq.1})$$

## 2.6. Determination of chemical constituents of essential oil

## 2.6.1. Spectrophotometric determination

All the essential oil samples were subjected to colorimetric assay for the determination of menthol (%) in *Mentha arvensis* L. as per the specifications mentioned in [16,17]. The standard equation obtained from standard curve of variable concentrations of GC-grade menthol was $y = 0.0185x + 0.0922$ with $R^2 = 0.989$.

## 2.6.2. Gas chromatographic analysis

After the spectrophotometric determination of menthol (%), some selected essential oil samples were subjected to gas chromatographic analysis using BK-$GC_{7820}$ Gas Chromatograph, Biobase, China as per the experimental protocol mentioned in [18].

## 2.7. Biological activities

## 2.7.1. Total phenolic contents (TPC)

The TPC of aqueous extracts of *Mentha arvensis* L. were determined by experimental protocols as mentioned in [19]. The standard equation obtained by standard curve of gallic acid for the assessment of TPC was $\mathrm{y} = 0.0137\mathrm{x} + 0.2987$ with $\mathrm{R}^2 = 0.9897$.

## 2.7.2. Total flavonoid contents (TFC)

The TFC of aqueous extracts of *Mentha arvensis* L. were determined by experimental protocols as mentioned in [19]. The standard equation obtained by the standard curve of catechin for the assessment of TFC was $\mathrm{y} = 0.0044\mathrm{x} - 0.0566$ with $\mathrm{R}^2 = 0.989$.

## 2.7.3. DPPH free radical scavenging activity

The DPPH free radical scavenging potentials of aqueous extracts of *Mentha arvensis* L. were determined by experimental protocols as mentioned in [19]. The DPPH free radical scavenging potentials (%) were calculated as per the following formula (Eq. 2):

$$\mathrm{DPPH scavenging activity}\,(\%) = 100 - \left[\frac{\mathrm{Sample absorbance}}{\mathrm{Control absorbance}}\right] \times 100 \ldots\ldots\ldots \mathrm{Eq.\,2}$$

## 2.7.4. Reducing power ability (RPA)

The RPA of aqueous extracts of *Mentha arvensis* L. were determined by experimental protocols as mentioned in [19]. The standard equation obtained by the standard curve of gallic acid for the assessment of RPA was $\mathrm{y} = 0.0114\mathrm{x} - 0.0455$ with $\mathrm{R}^2 = 0.989$.

# 2.8. Assessment of physiochemical characteristics

## 2.8.1. Photodegradation

The photodegradation profiles of 28-homobrassinolide, ethephon and their corresponding NPs were determined by exposing the 250 ppm solutions to the natural sunlight, for about 8 to 10 hours daily at 35°C upto 28 days. The UV-Vis spectra were recorded from 340 to 800 nm at (i) day 0 (ii) day 1 (iii) day 3 (iv) day 5 (v) day 7 (vi) day 14 and (vii) day 28, using 721(D) spectrophotometer, China [20–22].

## 2.8.2. Thermal degradation

The thermal degradation profiles of 28-homobrassinolide, ethephon and corresponding NPs were determined by heating the 250 ppm solutions at variable temperatures ranges for 8 to 10 hours daily. The UV-Vis spectra were recorded from 340 to 800 nm at (i) 30°C (ii) 35°C (iii) 40°C (iv) 45°C (v) 50°C (vi) 55°C and (vii) 60°C, using 721(D) spectrophotometer, China [23,24].

## 2.8.3. Leaching potential

The leaching potentials of 28-homobrassinolide, ethephon and their corresponding NPs were determined by adding the 50 mL of 250 ppm solution in a glass column, having the internal diameter of 20 mm, filled with sand (particle size: 0.05 mm to 2.00 mm), silt (particle size: 0.002 mm to 0.05 mm) and clay (particle size:  0.002 mm). The standard equations obtained from standard curves of 28-homobrassinolide, ethephon and their corresponding NPs at variable concentrations were having$\mathrm{R}^2 > 0.99$. The obtained leachate solutions were also analyzed by 721(D) spectrophotometer, China at the $\lambda_{max}$ of NPs [25].

## 2.8.4. MTT cytotoxic assay

### 2.8.4.1. Isolation of living cells

The MTT cytotoxic assay was performed by isolating the living cell suspensions from healthy leaves of *Mentha arvensis* L. as per experimental protocols mentioned in [26].

## 2.8.4.2. Method of preparation of negative control (NC)

The negative control was prepared by obtaining the standard equation from standard curve $(\mathrm{y} = 0.0441\mathrm{x} + 0.481 \mathrm{with} \mathrm{R}^2 = 0.9914)$ using the variable concentration of living cell suspensions as per the experimental protocols mentioned in [27].

## 2.8.4.3. Method of preparation of positive control (PC)

The positive control was prepared by adding variable concentrations of nanostructured PGRs (25, 50, 75, 100, 125, 150, 175, 200, 225 and 250 ppm) in 2 µL of living cell suspensions, followed by the shaking at 200 rpm. All the next steps were according to the experimental protocols as mentioned in [27,28]. The viable cell concentrations (%) were calculated according to the following equation (Eq. 3):

$$\mathrm{Cellviability}\,(\%) = \frac{\mathrm{PC}_{(\mathrm{Absorbance})} - \mathrm{NC}_{(\mathrm{Absorbance})}}{\mathrm{PC}_{(\mathrm{Absorbance})}} \times 100 \ldots\ldots\ldots (\mathrm{Eq.3})$$

# 2.9. Characterization techniques

## 2.9.1. Fourier transform infrared spectroscopy (FTIR)

The functional groups of 28-homobrassinolide, ethephon and their corresponding NPs were determined by using the Agilent Cary 630 FTIR spectrometer, USA as per the experimental protocols mentioned in [29].

## 2.9.2. Laser induced breakdown spectroscopy (LIBS)

The elemental analysis of 28-homobrassinolide, ethephon and their corresponding NPs was performed by using the LIBS: model Q-Smart 850 and NOVA Quantal, France as per the instrumental specifications and experimental protocols mentioned in [30].

## 2.9.3. Differential scanning colorimetry-thermogravimetric analysis (DSC-TGA)

The thermal stability of 28-homobrassinolide and ethephon was determined by using the SDT $Q_{600}$ $V_{20.9}$ Build 20, Crawley, UK as per the instrumental specifications mentioned in [31].

## 2.9.4. Scanning electron microscopy (SEM)

The surface characteristics and morphological properties of the 28-homobrassinolide-Ca-NPs and ethephon-Zn-NPs were determined by Nova NanoSEM 450, FEI, Oregon, USA as per the experimental protocols and instrumental specifications mentioned in [32].

## 2.9.5. Atomic absorption spectroscopy (AAS)

The trace metal analysis of 28-homobrassinilide-Zn-NPs and ethephon-Zn-NPs were performed by using Z-8200 polarized Zeeman atomic absorption spectrophotometer (AAS) Hitachi, Japan with instrumental

specifications as mentioned in [33].

## 2.10. Statistical analysis

The highest menthol (%) of *Mentha arvensis* L., grown by applying the three different concentrations (low: 25 ppm (Level-I), medium: 100 ppm (Level-II) and high: 250 ppm (Level-III)) of nanostructured PGRs were statistically compared by using ANOVA along with post-hoc Tukey HSD test [34].

# 3. Results and discussion

## 3.1. Physical attributes and percentage yield of essential oil

In the present study, *Mentha arvensis* L. was grown by the application of nanostructured PGRs (EDTA-NPs, Si-NPs, Ca-NPs and Zn-NPs) at three different dose concentrations [Level-I: 25 ppm, Level-II: 100 ppm and Level-III: 250 ppm], to check their effects on the yield and menthol (%) of essential oil. The results of present study showed that the essential oil yield of *Mentha arvensis* L., grown by applying the above mentioned nanoformulations ranged from 0.92 ± 0.09 to 0.65 ± 0.09%. The highest essential oil yield was obtained by the *Mentha arvensis* L., grown by the application of 28-homobrassnolide-Zn-NPs-L-II as brassinosteroids and all the structural analogues are known to have significant influence on the physiological attributes and biochemical processes of aromatic medicinal plants. These steroidal hormones have been reported to regulate the photosynthetic processes [35] and catalytic potentials of several enzymes [36].

According to [37], the foliar sprays of $10^{-7}$ M 28-homobrassinolide remarkably increased the percentage of menthyl acetate (225.0–187.5%), menthol (135.9–134.1%) and menthone (180.0–161.1%) in the essential oil of *Mentha arvensis* L. It has also been reported by [38] that *Mentha arvensis* L. showed higher biomass yield and improved essential oil (%) (including menthol, L-menthone, isomenthone and menthyl acetate) at $10^{-7}$ M concentration of 28-homobrassinolide as compared to the lower ($10^{-6}$ M) and higher ($10^{-8}$ M) concentrations. In addition to the plant growth regulator (PGR), Zn-NPs itself acts as an important growth promoter of the aromatic medicinal herbs, by enhancing the nutrient absorption capacity of number of essential macronutrients. In some previous studies, [39,40] reported the similar effects on essential oil contents of *Ocimum sanctum* and *Mentha piperita* by the exogenous application of zinc. In another study, [41] mentioned the 4.73% increase in menthol (%) in essential oil of menthol mint at 5.0 mg Zn $kg^{-1}$ application of doses.

## 3.2. Determination of chemical constituents of essential oil

### 3.2.1. Spectrophotometric determination

As per the results obtained by the present research, the menthol percentage of essential oil of *Mentha arvensis* L., grown by applying all the above mentioned nanoparticles were in the range of 81.93 ± 0.26 to 54.01 ± 0.04%. The highest menthol contents were obtained by the essential oil of *Mentha arvensis* L.,

grown by the application of ethephon-Zn-NPs-L-II as ethylene releasing auxin based compounds shows positive synergism in improving the production of menthol [9]. According to [42], the essential oil of peppermint showed significant increase in percentage of isomenthone and neoisomenthol by the foliar application of 250 ppm ethephon. Similarly, [43] mentioned the higher biosynthesis of terpenoids in *Cannabis sativa* L., upon exogenous application of 100 µM ethephon. As per the data reported by [9], ethephon provides abiotic stress to the aromatic plants and triggers the biosynthesis of abscisic acid, resulting in the higher production of essential oil. Additionally, Zn-NPs are also known to triggers the production and release of essential oil with higher menthol percentage as zinc activates the antioxidant enzymes and stress proteins under abiotic stresses such as excessive salt and severe water shortage [44].

# 3.2.2. Gas chromatographic analysis

The major and minor chemical constituents of essential oil of *Mentha arvensis* L., grown by applying the 28-homobrassinolide-Ca-NPs-L-III and ethephon-Zn-NPs-L-II are shown (Table 1). According to the gas chromatographic analysis, the l-menthol is a major chemical constituent of essential oil of *Mentha arvensis* L., with menthone, 1,8-cineol, eugenol, camphor, myrcene, α-pinene, γ-terpinene, linalool, borneol and d-menthol being the minor one. The menthol (%) of *Mentha arvensis* L., grown by the application of 28-homobrassinolide-Ca-NPs-L-III (82.18 ± 0.05%) and ethephon-Zn-NPs-L-II (84.64 ± 0.02%) is much higher as compared to the control (67.23 ± 0.13%) and blank (63.98 ± 0.16%). In a previous study, [45] also reported the higher menthol (38.27%) and menthone (29.87%) contents in essential oil of *Mentha piperita* L., by the exogenous application of 24-epibrassinolide (24-eBL). In another study, [37] reported the 135.9% increase in the menthol production in corn mint (*Mentha arvensis* L.), by the foliar application of three different plant growth regulators (PGRs) including the 28-homobrassinolide.

Table 1
Gas chromatographic analysis of essential oil of *Mentha arvensis* L.

| Sr. No | Chemical constituents | Essential oil of *Mentha arvensis* L. grown with the application of PGRs | | | |
|---|---|---|---|---|---|
| | | 28-Homobrassinolide-Ca-NPs-L-III | Ethephon-Zn-NPs-L-II | Control treatment | Blank |
| | | Percentage composition of chemical constituents | | | |
| **Major Chemical Constituents** | | | | | |
| 1 | l-Menthol | 82.18 ± 0.05 | 84.64 ± 0.02 | 67.23 ± 0.13 | 63.98 ± 0.16 |
| 2 | Menthone | 0.07 ± 0.07 | 0.0009 ± 0.09 | 4.45 ± 0.04 | 0.94 ± 0.04 |
| 3 | 1,8-Cineol | 0.60 ± 0.04 | 2.69 ± 0.01 | 10.11 ± 0.05 | 2.59 ± 0.01 |
| **Minor Chemical Constituents** | | | | | |
| 1 | Eugenol | 0.05 ± 0.01 | 0.003 ± 0.04 | 1.03 ± 0.03 | 1.71 ± 0.05 |
| 2 | Camphor | 0.07 ± 0.04 | 0.0009 ± 0.02 | 2.69 ± 0.07 | 1.31 ± 0.08 |
| 3 | Myrcene | 16.40 ± 0.05 | 5.50 ± 0.04 | 3.91 ± 0.06 | 22.99 ± 0.03 |
| 4 | α-Pinene | 0.13 ± 0.08 | 0.12 ± 0.02 | 0.06 ± 0.15 | 0.95 ± 0.02 |
| 5 | γ-Terpinene | 0.18 ± 0.09 | 1.03 ± 0.09 | 1.78 ± 0.10 | 0.89 ± 0.06 |
| 6 | Linalool | 0.05 ± 0.02 | 0.39 ± 0.05 | 2.81 ± 0.03 | 3.94 ± 0.10 |
| 7 | Borneol | 0.29 ± 0.01 | 5.34 ± 0.01 | 5.93 ± 0.08 | 0.56 ± 0.06 |
| 8 | d-Menthol | 0.0004 ± 0.03 | 0.29 ± 0.08 | 0.0023 ± 0.07 | 0.14 ± 0.09 |
| **Total Percentage** | | 100.00 | 100.00 | 100.00 | 100.00 |

In some previous researches, [42,46–48] also reported the highly positive effects of ethephon (Phosfon D) sprays on the essential oil production and menthol (%) of different aromatic plants. In addition to the PGRs, zinc has also been reported to enhance the biosynthesis of menthol in herbaceous plants [41,49,50]. In addition to the l-menthol, some exceptions have been observed in other chemical constituents of essential oil of *Mentha arvensis* L., such as (a) 28-homobrassinolide-Ca-NPs-L-III (myrcene: 16.40 ± 0.05%) (b) ethephon-Zn-NPs-L-II (borneol: 5.34 ± 0.01%) (c) control (menthone: 4.45 ± 0.04%, 1,8-cineol:

10.11 ± 0.05% and myrcene: 5.93 ± 0.08%) and (iv) blank (myrcene: 22.99 ± 0.03% and linalool: 3.94 ± 0.10%). According to the [2], these variations in the essential oil constituents might also be due to the climatic conditions, seasonal variations and number of biotic and abiotic stresses, capable of altering the biosynthetic pathways of aromatic medicinal herbs.

# 3.3. Biological activities

## 3.3.1. Total phenolic contents (TPC)

The results of present study showed that the total phenolic contents of aqueous extracts of *Mentha arvensis* L., grown by applying the different types of nanoformulations ranged from 50.41 ± 0.02 to 33.11 ± 0.03 mg/L of GAE. The highest total phenolic contents were obtained by the *Mentha arvensis* L., grown by the application of ethephon-Si-NPs-L-I as ethylene releasing compounds have been reported to enhance the production of phenols in plants. According to [51], the exogenous application of ethephon caused 82% and 20% increase in anthocyanins and 24 hydroxycinnamic acid in hairy root cultures of black carrot. It has also been reported by [52] that foliar application of ethephon remarkably increased the total phenolic contents in tempranillo grapes. It has been reported by [53] that 1000 ppm solution of ethephon increased the total phenolic contents of *Citrus limon* L. According to the [54], *Beta vulgaris* L. exhibited the higher production of total phenolic contents by applying the ethephon. In addition to the ethephon, some additional impacts might also be attributed to the presence of silica nanoparticles as silica possesses enough potential to alter the hormonal system of plants. The [55] holds the view that silica improved the catalytic potential of glucose-6-phosphate dehydrogenase in Mung bean sprouts.

## 3.3.2. Total flavonoid contents (TFC)

In the present study, the aqueous extracts of *Mentha arvensis* L., grown by applying all the above mentioned nanoformulations showed the total flavonoid contents ranging from 136.36 ± 0.01 to 14.12 ± 0.12 mg/L of CE. The highest total flavonoid contents were obtained by the aqueous extract of *Mentha arvensis* L., grown by the application of 28-homobrassonolide-L-II because moderate level of plant growth regulators can trigger the biosynthesis of secondary metabolites, by altering the physiological responses in *Lamiaceae*[56]. According to [57], 1.0 mg $L^{-1}$ dose concentration of 24-epibrassinolide (24-eBL) produced the highest flavonoid contents in transgenic hairy roots of *Echinacea purpurea* L. Moench. There are also some evidences to suggest that 0.0 to 0.5 µM dose concentration of 24-epibrassinolide (EBL) can trigger the production of secondary metabolites in dragonhead (*Dracocephalum moldavica* L.) [58]. Many scholars hold the view that 28-homobrassinolide and all the structural analogues can reduce the biotic and abiotic stresses in medicinal plants by altering the hormonal responses and producing the higher quantities of antioxidant compounds [59–62].

## 3.3.3. DPPH free radical scavenging activity

The obtained results showed that DPPH free radical scavenging potentials (%) of aqueous extracts of *Mentha arvensis* L., grown by applying the above mentioned PGRs ranged from 87.78 ± 0.17 to 20.25 ±

0.06%. Both the 28-homobrassonolide-Si-NPs-L-I and 28-homobrassonolide-Zn-NPs-L-III showed the significant improvements in DPPH free radical scavenging potentials because the additional input of brassinosteroids (as steroidal hormones) stimulate the production of osmotic constituents and antioxidant compounds in plants. It also regulates the phytohormones and stress responses in aromatic medicinal herbs [63]. It has been reported that exogenous application of homobrassinolide enhanced the DPPH free radical scavenging potentials of methanolic extracts of *Mentha arvensis* L. upto 35.83% [64]. The findings of present research work are also supported by the [65], dealing with the solvent based extraction (combination of ethylene glycol and choline chloride as deep eutectic solvents) of antioxidant compounds. According to [35], higher concentrations of 28-homobrassinolide can enhance the DPPH free radical scavenging activities of *Mentha arvensis* L., due to the increased catalytic potentials of carbonic anhydrases.

### 3.3.4. Reducing power ability (RPA)

In the present research work, the reducing power abilities of aqueous extracts of *Mentha arvensis* L., grown by applying the above mentioned nanoformulations ranged from 92.37 ± 0.23 to 16.55 ± 0.01 mg/L of GAE. The highest reducing power ability was exhibited by the aqueous extract of *Mentha arvensis* L., grown by application of ethephon-L-I as the lower concentrations of ethylene releasing compounds trigger the hormonal system of plants, responsible for producing the antioxidants and phytochemicals [66]. According to [67], *Solanum melongena* L. also showed the significant variations in antioxidant compounds by the exogenous application of 0.15% 2-CEPA (ethephon). According to recent research, exogenously applied ethylene releasing ethephon (2-chloroethyl phosphonic acid) significantly improved the antioxidant enzymatic system and number of photosynthetic processes in rice (*Oryza sativa* L.) [68]. There is another evidence to suggest that ethephon (source of ethylene) induces higher production of secondary metabolites, more specifically antioxidant compounds in black carrot hairy root culture [51].

## 3.4. Assessment of physiochemical characteristics

### 3.4.1. Photodegradation

The photodegradation profiles of nanostructured PGRs showed that almost all the NPs are highly photo-stable. All these chemical compounds showed no change in the UV-Vis spectra ranging from 340 to 800 nm, indicating the longer shelf-life with maintenance of actual structure. Only the small changes were observed in the UV-Vis spectrum of ethephon-Zn-NPs ranging from 340 to 380 nm. These effects might be attributed to the π→π* and n→π* transitions of phosphorous based functional groups of ethephon. As per the data obtained by "Environmental Protection Agency" (EPA), the ethephon ($C_2H_6ClO_3P$) is a highly resistant compound of nature, and shows only slight structural variations when come in contact with the living organisms of soil, under aerobic conditions [69]. However, ethephon-Zn-NPs showed only slight variations and these effects can be due to the additional input of nanostructured zinc. In a recently

conducted research, [70] mentioned the significant improvements in thermal stabilities, chemical characteristics and photocatalytic properties of zinc at nanoscale.

## 3.4.2. Thermal degradation

Thermaldegradation profile of ethephon, ethephon-Si-NPs and ethephon-Zn-NPs are shown (Fig. 1). The thermal degradation profiles of nanostructured PGRs showed that all the nanoformulations are highly thermally stable except for the few as mentioned here in detail. The UV-Vis spectrum of ethephon showed minor variations, ranging from 340 to 400 nm, due to the release of ethylene gas. In a previous research article, [71] reported the higher thermal stabilities of ethylene releasing plant growth inhibitors that lead to the formation of di-hydrogen phosphate under alkaline conditions. In case of ethephon-EDTA-NPs, only slight fluctuations were observed in the UV-Vis spectrum ranging from 340 to 390 nm. However, these transitions are very less as compared to the pure ethephon, due to the higher thermal stabilities of EDTA-NPs. In a previously published research, [72] reported the higher thermal stability of EDTA due to its degradation temperature ranging from 200 to 260°C. During the decomposition of EDTA, only the ethylenic bond (C–N) breaks to produce the two stable compounds including the (i) N-(2-hydroxyethyl)iminodiacetic acid and (ii) iminodiacetic acid.

Similarly, the UV-Vis spectrum of ethephon-Si-NPs also showed some variations in the pattern ranging from 340 to 540 nm. These minor changes indicated the higher thermal stability of silica based nanoformulations. In a recently conducted research, [73] reported the higher thermal stability of calcium silicate hydrate ($CaO\text{-}SiO_2\text{-}Cr(NO_3)_3\text{-}H_2O$) upto 550°C. The calcium silicate hydrate are thermally stable up-till 500°C, and starts to change the physical properties and chemical composition at the temperature greater than 550°C. In the case of ethephon-Zn-NPs, slight variations were observed in the UV-Vis spectrum ranging from 340 to 390 nm. However, these variations were less pronounced as compared to the ethephon, due to the presence of Zn-NPs. In a previously conducted research, [74] reported the higher thermal stabilities of zinc sulphate heptahydrate ($ZnSO_4.7H_2O$) upto 120°C. This molecule only shows the slight variations in the weight, due to the loss of water molecules, at a temperature ranging from 70 to 120°C. By further heating the compound till 260°C, more weight loss was due to the release of sulphate ions from zinc sulphate.

## 3.4.3. Leaching potential

The leaching potentials of 28-homobrassinolide, ethephon, 28-homobrassinolide-EDTA-NPs, ethephon-EDTA-NPs, 28-homobrassinolide-Si-NPs, ethephon-Si-NPs and 28-homobrassinolide-Ca-NPs were according to the pore size and empty spaces of soil media. However, some exceptions were observed in the ethephon-Ca-NPs, 28-homobrassinolide-Zn-NPs and ethephon-Zn-NPs. In all these above mentioned nanoformulations, silt showed more affinity for the nanostructured PGRs as compared to the clay particles. In the case of ethephon-Ca-NPs, the ethephon showed lower leaching potentials and higher binding affinities with the silt grains, due to the bond formation in between calcium oxide and silicon oxide as reported in previous research [75]. In the case of zinc based nanoformulations, both 28-homobrassinolide-Zn-NPs and ethephon-Zn-NPs showed maximum retention inside the glass column,

with the minimum wastage of all applied chemicals. These effects might be attributed to the fact that zinc can form the divalent cations and chelated metal ions when found in aqueous suspension, resulting in the formation of larger complexes [76].

# 3.4.4. MTT cytotoxic assay

The obtained result showed that the average cell survival rate of *Mentha arvensis* L., treated with the 28-homobrassinolide and ethephon based nanoformulations was 74.28 ± 0.02 and 74.80 ± 0.03%, respectively. The order of viable cell concentration (%) was as follows: (a) 28-homobrassinolide-Zn-NPs (75.10 ± 0.37) > 28-homobrassinolide-Si-NPs (75.01 ± 0.27) > 28-homobrassinolide-Ca-NPs (74.70 ± 0.30) > 28-homobrassinolide (74.08 ± 0.59) > 28-homobrassinolide-EDTA-NPs (72.52 ± 0.28%) and (b) ethephon-Si-NPs (78.02 ± 0.35) > ethephon (74.85 ± 1.61) > ethephon-Ca-NPs (74.16 ± 0.47) > ethephon-Zn-NPs (73.64 ± 0.82) > ethephon-EDTA-NPs (73.31 ± 0.54%). In a previous study, [77] recommended the $10^{-7}$ M homobrassinolide spray on *Mentha arvensis* L., along with the other plant growth regulators such as triacontanol and irradiated sodium alginates. In another study, [37] also reported the $10^{-7}$ M 28-homobrassinolide to be optimum for the *Mentha arvensis* L.

In a previously published article, [38] used the variable concentrations of 28-homobrassinolide ($10^{-0}$, $10^{-8}$, $10^{-7}$ and $10^{-6}$ M) and reported the highest menthol (%) by applying $10^{-7}$ M 28-homobrassinolide. In another research work, [45] mentioned the use of 0.5, 1.5 and 2.5 ppm solutions of 24-epibrassinolide (24-eBL) on the *Mentha piperita* L. In the previously conducted research, [42] used the 250 ppm solution of ethephon on the *Mentha arvensis* L. (peppermint), and reported the significant reduction in essential oil (%). In another article, [78] used 0.06% ethephon (2-chloroethyl phosphonic acid) on the Japanese mint and claimed the insignificant variations on the essential oil contents. In another research work, [43] used 1 to 100 µM ethephon solution on the *Cannabis sativa* L. and reported the significant variations in essential oil contents, by varying the concentration of PGRs.

# 3.5. Characterization techniques

# 3.5.1. Fourier transform infrared spectroscopy (FTIR)

The FTIR spectra of 28-homobrassinolide, ethephon and their corresponding NPs are shown (Fig. 2). In the FTIR spectrum of 28-homobrassinolide, the less dominant and weaker peaks at 1736.9 and 2079.9 $cm^{-1}$ were due to the C = O stretching vibrations and C–H bending vibrations of aromatic ringed structure. The tapered ended, dominant, sharp and strong peak at 1114.5 $cm^{-1}$ represented the C–O stretching vibrations of 28-homobrassinolide. In the fingerprint region of FTIR spectrum, the sharp and broad peaks at 674.6 and 868.5 $cm^{-1}$ represented the C = C bending vibrations, produced *via* liberation of methyl and hydroxyl groups [79]. In the FTIR spectra of 28-homobrassinolide based nanoformulations, only characteristic peaks are described in detail and rest of the peaks are according to the FTIR spectrum of 28-homobrassinolide. In the FTIR spectrum of 28-homobrassinolide-EDTA-NPs, the strong, broad and deep shouldered peak at 3019.1 $cm^{-1}$ indicated the strong stretching vibrations of N–H bonds of amines

and the broad and strong peak at 1632.6 $cm^{-1}$ represented the intense C = O stretching vibrations. The two broad and strong peaks at 1043.7 and 1114.5 $cm^{-1}$ were due to the C–N and C–O stretching vibrations, respectively [80].

In the FTIR spectrum of 28-homobrassinolide-Si-NPs, the broad and a strong peak at 1080.9 $cm^{-1}$ was due to the S = O stretching vibrations and two simultaneous peaks at 648.6 and 998.9 $cm^{-1}$ were caused by the weak O–Si–O and strong C = C bending vibrations, respectively [81]. In the FTIR spectrum of 28-homobrassinolide-Ca-NPs, a strong peak at 1628.8 $cm^{-1}$ showed the stretching vibrations of C = O bond, and a pair of peaks at 1423.8 and 1483.5 $cm^{-1}$ were due to the combined effects of stretching vibrations of strong Ca–O bond and strong bending vibrations of –OH groups. In addition, two individual peaks at 883.4 and 1110.7 $cm^{-1}$ were due to the weak Ca–O bond and strong C–O stretching vibrations [82]. In the FTIR spectrum of 28-homobrassinolide-Zn-NPs, five individual peaks at 451, 667.2, 745.5, 872.2 and 1084.7 $cm^{-1}$ were due to the strong ZnO bond, C = C bending vibrations and stretching and bending vibrations of $SO_4^{-2}$ ions [74].

In the FTIR spectrum of ethephon, five sharp, weak and simultaneous peaks at 3000.5, 3213.0, 3309.9, 3406.8 and 3526.1 $cm^{-1}$ indicated the strong stretching vibrations of –OH groups, due to the presence of intra-molecularly bonded alcoholic functional groups. In the next portion, two weak and broad peaks at 2703.3 and 2914.8 $cm^{-1}$ were caused by the –OH and C–H stretching vibrations. Just before the fingerprint region of FTIR spectrum, the broad and strong peak at 1654.9 $cm^{-1}$, and sharp and weak peak at 1751.8 $cm^{-1}$ were caused by the stretching vibrations of carbonyl groups. In the next portion, two sharp and strong peaks at 1438.8 and 1498.4 $cm^{-1}$ were mainly attributed to the C–H bending vibrations, due to the presence of methylene functional groups. In this series, some multiple peaks at 1222.6, 1271.0, 1312.0 and 1386.6 $cm^{-1}$ were due to the stretching vibrations of P–O and P = O, indicating the presence of phosphate functional groups. Some additional pointed and sharp peaks at 820.0, 719.4 and 752.9 $cm^{-1}$ were caused by the strong stretching vibrations of C–Cl bonds. Similarly, some multiple peaks at 674.6, 868.5 and 987.7 $cm^{-1}$, and 1021.3, 1056.0 and 1110.7 $cm^{-1}$ were due to the C = C and C–H bending vibrations and C–O stretching vibrations, respectively [83]. In the FTIR spectra of ethephon based nanoformulations, only characteristic peaks are described in detail and rest of the peaks are according to the FTIR spectrum of ethephon.

In the FTIR spectrum of ethephon-EDTA-NPs, two sharp and weak peaks at 3015.4 and 3526.1 $cm^{-1}$, and two merged and broad peaks at 3313.6 and 3406.8 $cm^{-1}$ were caused by the N–H and –OH stretching vibrations. In addition, a pointed, broad and strong peak at 1654.9 $cm^{-1}$ and a sharp and shouldered peak at 7151.8 $cm^{-1}$ were due to the C = O stretching vibrations [80]. In the FTIR spectrum of ethephon-Si-NPs, two pointed, sharp and weak peaks at 652.3 and 872.2 $cm^{-1}$ were mainly attributed to the presence of O–Si–O and Ca–O bonds, respectively [81]. In the FTIR spectrum of ethephon-Ca-NPs, two broad and strong peaks at 1319.3 and 1565.5 $cm^{-1}$ and a sharp, medium peak at 1722.0 $cm^{-1}$ were due to the combined effects of stretching vibrations of P–O and P = O bonds and weak Ca–O bonds of reacting

molecules, and stretching vibrations of C = C and C = O bonds, indicating the release of chlorine atoms from ethylene-releasing-compounds. Similarly, a pointed, sharp and independent peak at 872.2 $cm^{-1}$ was mainly caused by the Ca–O bond stretching vibrations [82]. In the FTIR spectrum of ethephon-Zn-NPs, some pointed, sharp and singlet peaks at 451 and 652.3 $cm^{-1}$ were due to the ZnO stretching vibrations and fundamental vibrations of $SO_4^{-2}$ ions. In the next portion, some multiple peaks at 1121.9 and 1155.5 $cm^{-1}$ and 1358.8 and 1408.9 $cm^{-1}$ were due to the fundamental vibrations of $SO_4^{-2}$ ions and strong S = O stretching vibrations, respectively [74].

## 3.5.2. Laser induced breakdown spectroscopy (LIBS)

The LIBS spectra of 28-homobrassinolide, ethephon and their corresponding NPs are shown (Fig. 3). The elemental analysis of all above mentioned samples was made possible by obtaining the emitted wavelengths of analytical samples during the atomic transitions. These transitions were recognized by the use of NIST (National Institute of Standard and Technology) data base. Some of the major and minor identified elements were as follows: (a) 28-homobra-ssinolide: C(III) and O(II) (b) ethephon: Cl(I), O(II) and Cl(II) (c) 28-homobrassinolide-EDTA-NPs: Na(I), C(II), Cl(I), N(II) and O(II) (d) ethephon-EDTA-NPs: C(II), Na(II), O(II), Na(I), Cl(II) and C(I) (e) 28-homobrassinolide-Si-NPs: C(II), Ca(I), Si(II), O(V), C(I), Ca(I), Cl(I), S(III), S(II), Cl(III), Ca(II), Na(II), Ca(III) and O(II) (f) ethephon-Si-NPs: C(I), Ca(III), Cl(I), O(IV), S(II), Cl(III), Na(II) and Ca(II) (g) 28-homobrassinolide-Ca-NPs: C(II), N(III), C(I), Ca(I), Na(II), N(II), O(II), Ca(II), Na(I) and Ca(III) (h) ethephon-Ca-NPs: C(I), Ca(III), Cl(I), O(IV), Cl(III), Ca(II) and Na(II) (i) 28-homobrassinolide-Zn-NPs: C(II), O(II), Na(II), Na(I), S(II), N(II) and S(III) and (j) ethephon-Zn-NPs: C(II), N(III), Ca(III), Cl(I), S(II), N(II), S(III), O(IV), Na(II), C(I) and Zn(II) [84].

## 3.5.3. Differential scanning colorimetry-thermogravimetric analysis (DSC-TGA)

The DSC-TGA curves of 28-homobrassinolide and ethephon are shown (Fig. 4). The thermal analyses were performed to check the range of degradation temperature of 28-homo-brassinolide and ethephon, prior to the preparation of nanostructured PGRs. The DSC-TGA curves were obtained by heating the PGRs upto 300°C, to check the gradual weight loss with respect to temperature. The thermogram obtained by the 28-homobrassinolide showed no weight loss till 50°C, only 15% weight loss till 150°C and again no weight loss up-till 300°C. At the temperature greater than 300°C, the exothermic reaction of thermal pyrolysis dominated and lead to the sudden weight loss upto 92 to 98%, as reported for brassinosteroid-modified polyethylene glycol micelles and various other structural analogues [85,86]. In case of DSC-TGA curves of ethephon, the thermogram showed no change in the weight till 200°C, only 35% weight loss till 230°C and almost 20% weight loss till 300°C. In a previous study, [87] reported the melting of ethephon at 73.3°C and thermal decomposition upto 250 to 400°C.

## 3.5.4. Scanning electron microscopy (SEM)

The SEM images of 28-homobrassinolide-Ca-NPs and ethephon-Zn-NPs are shown (Fig. 5). The SEM images of 28-homobrassinolide-Ca-NPs showed that the average particle size of prepared formulations ranged from 100 nm to 5 µm, having ovoid to spherical and irregular shape. The black spots and empty spaces in the SEM images are representative of the higher surface area to volume ratio, indicating the better assimilation of nanostructured PGR in the roots of *Mentha arvensis* L. These types of nanoformulations have not been reported yet, however literature strongly supports the obtained results and surface morphologies, with respect to the calcium based nanofertilizers. The edgy structure, hollow areas, dark spots, and smaller particle size are some of the major characteristic features, responsible for the slow release of attached water molecules. These types of nanoformulations have proved to be the ideal candidate for the geographical areas, having restricted availability of water. In some recently published research articles, [88–90] reported the significant improvements in surface properties and water holding capacities of nanoparticles, as compared to their bulk counterparts. In another previous research article, [91] also reported the larger surface area and improved characteristic properties of calcium oxide nano-particles due to the higher rate of agglomeration.

The SEM images of ethephon-Zn-NPs showed that the nanoparticles ranged from 100 nm to 5 µm, having hexagonal to columnar and cuboidal to diamond like shape. The small particle size and large empty spaces are the major characteristic features of zinc based nanoformulations [92]. In a recently published research article, [93] reported the spherical shape carbon balls enclosing the zinc sulphate nano-hybrids, for the fast and efficient delivery of zinc in the *Oryza sativa* L. In another research, [94] reported the spherical shape of ZnO nanoparticles, as a remedy for the rice crops. In a recent research article, [95] also used the zinc sulphate ($ZnSO_4$) nanoparticles on coffee (*Coffea arabica* L.). In a previous research work, [96] reported the spherical and merged balls of zinc oxide nanoparticles, prepared *via* microwave assisted method. In another article, [97] mentioned the spherical aggregated ZnO nanoparticles having particle size of 1 µm, prepared through green synthesis using *Hibiscus rosa-sinensis*.

# 3.5.5. Atomic absorption spectroscopy (AAS)

The zinc sulphate is a micro-nutrient of plants, having lower concentration (0.00022 g/L) as compared to the various other macro-nutrients and complexing agents. During the elemental analysis *via* LIBS, zinc was found to be below the detectable range of AvaSpec spectrometer. Therefore, the obtained concentrations of zinc were detected by the AAS. The results showed that the obtained concentrations of zinc in 28-homobrassinolides-Zn-NPs and ethephon-Zn-NPs were 0.125 ± 0.07 and 0.141 ± 0.14 ppm, respectively. These results were comparable with the added concentrations of zinc as per the previously published research article [40]. The slight variations in the final concentrations of zinc might be attributed to the leaching of Zn-NPs, during the process of washing and filtration.

# 3.6. Statistical analysis

The highest menthol (%) of *Mentha arvensis* L., grown by the application of 28-homobrassinolide-L-I (79.72%), 28-homobrassinolide-EDTA-NPs-L-I (79.58%), 28-homobrassinolide-Si-NPs-L-I (54.9%), 28-

homobrassinolide-Ca-NPs-L-III (80.84%) and 28-homobrassinolide-Zn-NPs-L-III (72.58%), and ethephon-L-I (67.59%), ethephon-EDTA-NPs-L-III (68.06%), ethephon-Si-NPs-L-III (80.94%), ethephon-Ca-NPs-L-III (81.53%) and ethephon-Zn-NPs-L-II (81.93%) were statistically compared with the control (67.19%) and blank (63.93%) treatments. The p-values obtained by the one way analysis of variance (ANOVA) were less than 0.05, indicating the higher statistical variability among all the obtained percentages. The post-hoc Tukey HSD test also indicated the significant variations among the different pairs of treatments, in all the possible combinations [34].

# 4. Conclusions

The 28-homobrassinolide and ethephon are two effective biostimulants in enhancing the release of secondary metabolites and production of menthol in *Mentha arvensis* L. However, the prepared nano-structured formulations have proved to be more effective in stimulating the bio-synthesis of secondary metabolites in *Mentha arvensis* L., as compared to the pure PGRs. The highest essential oil percentage of *Mentha arvensis* L. was obtained by the application of 28-homobrassinolide-Zn-NPs-L-II and ethephon-Ca-NPs-L-III. The highest menthol contents of *Mentha arvensis* L. were obtained by the application of 28-homobrassinolide-Ca-NPs-L-III and ethephon-Zn-NPs-L-II.

# Declarations

### Ethical Approval

No human or animal subjects were involved during the present study.

### Competing interests

All authors declare that there is no conflict of interest.

### Authors' contributions

Farwa Nadeem; Research work and article writeup

Muhammad Asif Hanif; Supervision, study conception and design and manuscript proof-read.

Najla AlMasoud; Data interpolation and discussion

Taghrid S. Alomar; Statistical evaluation, Figures, and table preparation

Adnan Younis; data collection, analysis, manuscript proof-read.

### Funding

No funding received for the present study.

### Availability of data and materials

All data generated or analysed during this study are included in this published article.

### Acknowledgement

Princess Nourah bint Abdularahman University Researchers Supporting Project number (PNURSP2023R47), Princess Nourah bint Abdularahman University, Riyadh, Saudi Arabia.

# References

1. Zaid, A., Mohammad, F. & Fariduddin, Q. Plant growth regulators improve growth, photosynthesis, mineral nutrient and antioxidant system under cadmium stress in menthol mint (Mentha arvensis L.). Physiology and Molecular Biology of Plants 26, 25–39, doi:10.1007/s12298-019-00715-y (2020).
2. Soltanbeigi, A., Özgüven, M. & Hassanpouraghdam, M. B. Planting-date and cutting-time affect the growth and essential oil composition of Mentha × piperita and Mentha arvensis. Industrial Crops and Products 170, 113790, doi:https://doi.org/10.1016/j.indcrop.2021.113790 (2021).
3. Pergolizzi Jr, J., Taylor Jr, R., LeQuang, J. A., Raffa, R. & Group, N. R. The role and mechanism of action of menthol in topical analgesic products. Journal of clinical pharmacy and therapeutics 43, 313–319 (2018).
4. Markets, M. a. Essential Oils Market by Type (Orange, Lemon, Lime, Peppermint, Citronella, and Others), Application (Food & Beverage, Cosmetics & Toiletries, Aromatherapy, Home Care, Health Care), Method of Extraction, and Region – Global Forecast to 2026. Report Code: 5385 (2021).
5. MarketWatch. Menthol Market Share 2021, Size, Industry Growth by Global Major Companies Profile, Competitive Landscape and Key Regions 2027. (2021).
6. Rahimi, Y., Taleei, A. & Ranjbar, M. Changes in the expression of key genes involved in the biosynthesis of menthol and menthofuran in Mentha piperita L. under drought stress. Acta Physiologiae Plantarum 39, 203, doi:10.1007/s11738-017-2502-x (2017).
7. Jamwal, K., Bhattacharya, S. & Puri, S. Plant growth regulator mediated consequences of secondary metabolites in medicinal plants. Journal of Applied Research on Medicinal and Aromatic Plants 9, 26–38, doi:https://doi.org/10.1016/j.jarmap.2017.12.003 (2018).
8. Kaur, H. *et al.* 28-homobrassinolide regulates antioxidant enzyme activities and gene expression in response to salt- and temperature-induced oxidative stress in Brassica juncea. Scientific Reports 8, 8735, doi:10.1038/s41598-018-27032-w (2018).
9. Sun, Z.-Y. *et al.* A novel role of ethephon in controlling the noxious weed Ipomoea cairica (Linn.) Sweet. Scientific Reports 5, 11372, doi:10.1038/srep11372 (2015).
10. Simmons, S., Oelke, E., Wiersma, J., Lueschen, W. & Warnes, D. Spring wheat and barley responses to ethephon. Agron. J. 80, 829–834 (1988).

11. Sharma, K., Pasricha, V., Satpathy, G. & Gupta, R. K. Evaluation of phytochemical and antioxidant activity of raw Pyrus communis (l), an underexploited fruit. Journal of pharmacognosy and Phytochemistry 3 (2015).
12. Taneja, S. & Chandra, S. in *Handbook of herbs and spices* 366–387 (Elsevier, 2012).
13. Sajjad, Y., Jaskani, M. J., Asif, M. & Qasim, M. Application of plant growth regulators in ornamental plants: a review. Pakistan Journal of Agricultural Sciences 54 (2017).
14. Bui-Phuc, T., Nhu-Trang, T. & Cong-Hau, N. in *IOP Conference Series: Materials Science and Engineering.* 012039 (IOP Publishing).
15. Antony, B., Benny, M. & Kaimal, T. A Pilot clinical study to evaluate the effect of Emblica officinalis extract (Amlamax™) on markers of systemic inflammation and dyslipidemia. Indian Journal of Clinical Biochemistry 23, 378–381 (2008).
16. Anastasia-Sandu, A., Bîrzu, S., Ditu, I. & Bulgariu, L. Direct Determination of menthol using a simple spectrophotometric method. Bulletin of the Polytechnic Institute of Iasi, Section Chemistry and Chemical Engineering, 71–80 (2013).
17. Nadeem, F., Hanif, M. A., Bhatti, I. A. & Qadri, R. W. K. Improved Spectrophotometric Method for Fast and Accurate Quantitative Determination of Menthol in Essential Oils. Food Analytical Methods 15, 1575–1580, doi:10.1007/s12161-021-02202-1 (2022).
18. Lothe, N. B. *et al.* Maximizing yields and economics by supplementing additional nutrients for commercially grown menthol mint (Mentha arvensis L.) cultivars. Industrial Crops and Products 160, 113110 (2021).
19. Khan, M. M., Hanif, M. A. & Abraham, A. S. Variations in basil antioxidant contents in relation to deficit irrigation. Journal of Medicinal Plants Research 6, 2220–2223 (2012).
20. Da Silva, E. S., Burrows, H. D., Wong-Wah-Chung, P. & Sarakha, M. β-Cyclodextrin as a photostabilizer of the plant growth regulator 2-(1-naphthyl) acetamide in aqueous solution. Journal of Inclusion Phenomena and Macrocyclic Chemistry 79, 329–336 (2014).
21. Da Silva, E. S., Wong-Wah-Chung, P., Burrows, H. D. & Sarakha, M. Photochemical Degradation of the Plant Growth Regulator 2-(1-Naphthyl) acetamide in Aqueous Solution Upon UV Irradiation. Photochemistry and photobiology 89, 560–570 (2013).
22. Jose, J. K. & Kuttan, R. Antioxidant activity of Emblica officinalis. Journal of clinical biochemistry and nutrition 19, 63–70 (1995).
23. Haque, R. *et al.* Protective effects of Emblica officinalis Gaertn. in cyclophosphamide-treated mice. Human & experimental toxicology 20, 643–650 (2001).
24. Kim, H. J. *et al.* Influence of amla (Emblica officinalis Gaertn.) on hypercholesterolemia and lipid peroxidation in cholesterol-fed rats. Journal of nutritional science and vitaminology 51, 413–418 (2005).
25. Bandyopadhyay, S. K., Pakrashi, S. C. & Pakrashi, A. The role of antioxidant activity of Phyllanthus emblica fruits on prevention from indomethacin induced gastric ulcer. Journal of Ethnopharmacology 70, 171–176 (2000).

26. Sabu, M. & Kuttan, R. Anti-diabetic activity of medicinal plants and its relationship with their antioxidant property. Journal of ethnopharmacology 81, 155–160 (2002).
27. Nandi, P., Talukder, G. & Sharma, A. Dietary chemoprevention of clastogenic effects of 3, 4-benzo (a) pyrene by Emblica officinalis Gaertn. fruit extract. British journal of cancer 76, 1279–1283 (1997).
28. JOSE, J. K., KUTTAN, G., GEORGE, J. & KUTTAN, R. Antimutagenic and anticarcinogenic activity of Emblica officinalis Gaertn. Journal of clinical biochemistry and nutrition 22, 171–176 (1997).
29. Borba, K. R. *et al.* Non-invasive quantification of vitamin C, citric acid, and sugar in 'Valência'oranges using infrared spectroscopies. J. Food Sci. Technol. 58, 731–738 (2021).
30. Iftikhar, A., Jamil, Y., Nazeer, N., Tahir, M. S. & Amin, N. Optical Emission Spectroscopy of Nickel-Substituted Cobalt–Zinc Ferrite. Journal of Superconductivity and Novel Magnetism, 1–6 (2020).
31. Han, F., Yun, S., Zhang, C., Xu, H. & Wang, Z. Steel slag as accelerant in anaerobic digestion for nonhazardous treatment and digestate fertilizer utilization. Bioresource technology 282, 331–338 (2019).
32. Iqbal, B. *et al.* One-Pot Synthesis of Heterobimetallic Metal–Organic Frameworks (MOFs) for Multifunctional Catalysis. Chem. Eur. J. 25, 10490–10498 (2019).
33. Cunniff, P. Official Methods of Analysis Association of Official Analytical Chemists. *Washington, DC* (1990).
34. Montgomery, D. C. *Design and analysis of experiments*. (John Wiley & Sons, 2017).
35. Naeem, M., Idrees, M., Alam, M. M., Aftab, T. & Khan, M. M. A. Brassinosteroid-mediated enrichment in yield attributes, active constituents and essential oil production in Mentha arvensis L. Russian agricultural sciences 38, 106–113 (2012).
36. Fariduddin, Q., Hasan, S. A., Ali, B., Hayat, S. & Ahmad, A. Effect of modes of application of 28-homobrassinolide on mung bean. Turkish journal of biology 32, 17–21 (2008).
37. Naeem, M. *et al.* Modulation of physiological activities, active constituents and essential oil production of Mentha arvensis L. by concomitant application of depolymerised carrageenan, triacontanol and 28-homobrassinolide. Journal of Essential Oil Research 29, 179–188, doi:10.1080/10412905.2016.1213188 (2017).
38. Naeem, M. *et al.* Brassinosteroid-mediated enrichment in yield attributes, active constituents and essential oil production in Mentha arvensis L. Russian Agricultural Sciences 38, 106–113, doi:10.3103/S1068367412020176 (2012).
39. Akhtar, N., Sarker, M. A. M., Akhter, H. & Nada, M. K. Effect of planting time and micronutrient as zinc chloride on the growth, yield and oil content of Mentha piperita. Bangladesh Journal of Scientific and Industrial Research 44, 125–130 (2009).
40. Kanwal, N., Hanif, M. A., Khan, M. M., Ansari, T. M. & Khalil-ur-Rehman. Effect of micronutrients on vegetative growth and essential oil contents of Ocimum sanctum. J. Essent. Oil Bear. Pl. 19, 980–988 (2016).

41. Pande, P., Anwar, M., Chand, S., Yadav, V. K. & Patra, D. D. Optimal Level of Iron and Zinc in Relation to Its Influence on Herb Yield and Production of Essential Oil in Menthol Mint. Commun. Soil Sci. Plant Anal. 38, 561–578, doi:10.1080/00103620701215627 (2007).
42. El-Keltawi, N. E. & Croteau, R. Influence of ethephon and daminozide on growth and essential oil content of peppermint and sage. Phytochemistry 25, 1285–1288, doi:https://doi.org/10.1016/S0031-9422(00)81273-X (1986).
43. Mansouri, H., Salari, F., Asrar, Z. & Nasibi, F. Effects of ethephon on terpenoids in Cannabis sativa L. in vegetative stage. J. Essent. Oil Bear. Pl. 19, 94–102 (2016).
44. Umair Hassan, M. *et al.* The critical role of zinc in plants facing the drought stress. Agriculture 10, 396 (2020).
45. Çoban, Ö. & Baydar, N. G. Brassinosteroid modifies growth and essential oil production in peppermint (Mentha piperita L.). Journal of plant growth regulation 36, 43–49 (2017).
46. Farooqi, A. A. & Sharma, S. Effect of growth retardants on growth and essential oil content in Japanese mint. Plant growth regulation 7, 39–45 (1988).
47. Et-Keltawi, N. E. & Croteau, R. Influence of phosfon D and cycocel on growth and essential oil content of sage and peppermint. Phytochemistry 25, 1603–1606 (1986).
48. Sharafzadeh, S. & Zare, M. Influence of growth regulators on growth and secondary metabolites of some medicinal plants from Lamiaceae family. Adv. Environ. Biol 5, 2296–2302 (2011).
49. Jahani, F., Tohidi-Moghadam, H. R., Larijani, H. R., Ghooshchi, F. & Oveysi, M. Influence of zinc and salicylic acid foliar application on total chlorophyll, phenolic components, yield and essential oil composition of peppermint (Mentha piperita L.) under drought stress condition. Arabian Journal of Geosciences 14, 691, doi:10.1007/s12517-021-07024-3 (2021).
50. Misra, A. & Sharma, S. Critical Zn concentration for essential oil yield and menthol concentration of Japanese mint. Fertilizer research 29, 261–265, doi:10.1007/BF01052394 (1991).
51. Barba-Espín, G. *et al.* Ethephon-induced changes in antioxidants and phenolic compounds in anthocyanin-producing black carrot hairy root cultures. Journal of Experimental Botany 71, 7030–7045 (2020).
52. López, R. *et al.* Ethephon foliar application: Impact on the phenolic and technological Tempranillo grapes maturity. Journal of Food Science 86, 803–812 (2021).
53. Zhang, P. & Zhou, Z. Postharvest ethephon degreening improves fruit color, flavor quality and increases antioxidant capacity in 'Eureka' lemon (Citrus limon (L.) Burm. f.). Sci. Hortic. 248, 70–80, doi:https://doi.org/10.1016/j.scienta.2019.01.008 (2019).
54. Barba-Espin, G. *et al.* Preharvest application of ethephon and postharvest UV-B radiation improve quality traits of beetroot (Beta vulgaris L. ssp. vulgaris) as source of colourant. BMC Plant Biology 18, 316, doi:10.1186/s12870-018-1556-2 (2018).
55. Liu, H.-K., Cao, Y., Huang, W.-N., Guo, Y.-D. & Kang, Y.-F. Effect of ethylene on total phenolics, antioxidant activity, and the activity of metabolic enzymes in mung bean sprouts. European Food Research and Technology 237, 755–764, doi:10.1007/s00217-013-2048-0 (2013).

56. Assaf, M., Korkmaz, A., Karaman, Ş. & Kulak, M. Effect of plant growth regulators and salt stress on secondary metabolite composition in Lamiaceae species. South African Journal of Botany 144, 480–493, doi:https://doi.org/10.1016/j.sajb.2021.10.030 (2022).
57. Demirci, T., Çelikkol Akçay, U. & Göktürk Baydar, N. Effects of 24-epibrassinolide and l-phenylalanine on growth and caffeic acid derivative production in hairy root culture of Echinacea purpurea L. Moench. Acta Physiologiae Plantarum 42, 1–11 (2020).
58. Zaji, B., Khavari-Nejad, R. A., Saadatmand, S., Nejadsatari, T. & Iranbakhsh, A. Combined application of 24-Epibrassinolide and selenium improves essential oil content and composition of dragonhead (Dracocephalum moldavica L.). J. Essent. Oil Bear. Pl. 22, 893–902 (2019).
59. Ali, B., Hayat, S. & Ahmad, A. 28-Homobrassinolide ameliorates the saline stress in chickpea (Cicer arietinum L.). Environmental and experimental botany 59, 217–223 (2007).
60. Hasan, S., Hayat, S., Ali, B. & Ahmad, A. 28-Homobrassinolide protects chickpea (Cicer arietinum) from cadmium toxicity by stimulating antioxidants. Environmental pollution 151, 60–66 (2008).
61. Masidur Alam, M., Hayat, S., Ali, B. & Ahmad, A. Effect of 28-homobrassinolide treatment on nickel toxicity in Brassica juncea. Photosynthetica 45, 139–142 (2007).
62. Ali, B., Hayat, S., Hasan, S. A. & Ahmad, A. Effect of root applied 28-homobrassinolide on the performance of Lycopersicon esculentum. Sci. Hortic. 110, 267–273 (2006).
63. Ahanger, M. A., Ashraf, M., Bajguz, A. & Ahmad, P. Brassinosteroids regulate growth in plants under stressful environments and crosstalk with other potential phytohormones. Journal of Plant Growth Regulation 37, 1007–1024 (2018).
64. Dar, M. A., Masoodi, M. H., Wali, A. F., Mir, M. A. & Shapoo, N. S. Antioxidant potential of methanol Root extract of Mentha arvensis L. from Kashmir Region. Journal of Applied Pharmaceutical Science 4, 50 (2014).
65. Naseem, Z. *et al.* Ultrasound-assisted deep eutectic solvent–based extraction of phytochemicals from Mentha arvensis: optimization using Box-Behnken design. Biomass Conversion and Biorefinery, doi:10.1007/s13399-021-01617-4 (2021).
66. Iqbal, N., Umar, S., Per, T. S. & Khan, N. A. Ethephon increases photosynthetic-nitrogen use efficiency, proline and antioxidant metabolism to alleviate decrease in photosynthesis under salinity stress in mustard. Plant signaling & behavior 12, e1297000 (2017).
67. Rogach, V., Reshetnyk, K., Kuryata, V. & Rogach, T. Influence of gibberellin inhibitors on the accumulation and redistribution of various forms of carbohydrates and nitrogen-containing compounds in plants of Solanum melongena L. Biologija 66 (2020).
68. Gautam, H. *et al.* Exogenously-Sourced Ethylene Positively Modulates Photosynthesis, Carbohydrate Metabolism, and Antioxidant Defense to Enhance Heat Tolerance in Rice. International Journal of Molecular Sciences 23, 1031 (2022).
69. Chathuranga, T. & C Peiris, L. D. Chronic (90 days) oral toxicity assessment of ethephon, a commercially available fruit ripener in male wistar rats. (2019).

70. Lakshmipriya, T. & Gopinath, S. C. in *Nanoparticles in Analytical and Medical Devices* 1–29 (Elsevier, 2021).
71. CAO, H.-e., XIA, H., LU, P. & YU, P. Determination of Ethephon Residues in Bean Sprout Samples by Static Headspace Gas Chromatography [J]. Agrochemicals 4 (2011).
72. Sokhanvarian, K., Nasr-El-Din, H. A. & De Wolf, C. A. in *SPE European Formation Damage Conference & Exhibition.* (OnePetro).
73. Niuniavaite, D. *et al.* Microstructure, Thermal Stability, and Catalytic Activity of Compounds Formed in CaO-SiO2-Cr (NO3) 3-H2O System. Nanomaterials 10, 1299 (2020).
74. Saha, J. & Podder, J. Crystallization of zinc sulphate single crystals and its structural, thermal and optical characterization. Journal of Bangladesh Academy of Sciences 35, 203–210 (2011).
75. Bouhadja, M., Jakse, N. & Pasturel, A. Structural and dynamic properties of calcium aluminosilicate melts: a molecular dynamics study. The Journal of chemical physics 138, 224510 (2013).
76. Cakmak, I., McLaughlin, M. J. & White, P. (Springer, 2017).
77. Naeem, M. *et al.* Employing depolymerised sodium alginate, triacontanol and 28-homobrassinolide in enhancing physiological activities, production of essential oil and active components in Mentha arvensis L. Industrial Crops and Products 55, 272–279, doi:https://doi.org/10.1016/j.indcrop.2014.01.052 (2014).
78. Abad Farooqi, A. H. & Sharma, S. Effect of growth retardants on growth and essential oil content in Japanese mint. Plant Growth Regulation 7, 39–45, doi:10.1007/BF00121688 (1988).
79. Massey, A. P., Pore, V. S. & Hazra, B. G. New route for the synthesis of (22S, 23S)-28-homobrassinolide. *Synthesis* 2003, 0426–0430 (2003).
80. Jayaprakash, J., Srinivasan, N. & Chandrasekaran, P. Surface modifications of CuO nanoparticles using Ethylene diamine tetra acetic acid as a capping agent by sol–gel routine. Spectrochimica Acta Part A: Molecular and Biomolecular Spectroscopy 123, 363–368, doi:https://doi.org/10.1016/j.saa.2013.12.080 (2014).
81. Thompson, S. P., Day, S. J., Parker, J. E., Evans, A. & Tang, C. C. Fine-grained amorphous calcium silicate CaSiO3 from vacuum dried sol–gel – Production, characterisation and thermal behaviour. Journal of Non-Crystalline Solids 358, 885–892, doi:https://doi.org/10.1016/j.jnoncrysol.2011.12.080 (2012).
82. Abdolmohammadi, S. *et al.* Enhancement of Mechanical and Thermal Properties of Polycaprolactone/Chitosan Blend by Calcium Carbonate Nanoparticles. International Journal of Molecular Sciences 13, doi:10.3390/ijms13044508 (2012).
83. Li, S. *et al.* A gold nanoparticle-loaded molecularly imprinted switch sensor with high sensitivity to ethephon. Microchemical Journal 157, 105025 (2020).
84. Kramida, A., Olsen, K. & Ralchenko, Y. Nist libs database. *National Institute of Standards and Technology, US Department of Commerce* (2019).

85. Pérez Quiñones, J., Brüggemann, O., Kjems, J., Shahavi, M. H. & Peniche Covas, C. Novel Brassinosteroid-Modified Polyethylene Glycol Micelles for Controlled Release of Agrochemicals. J. Agric. Food Chem. 66, 1612–1619, doi:10.1021/acs.jafc.7b05019 (2018).
86. Quiñones, J. P., García, Y. C., Curiel, H. & Covas, C. P. Microspheres of chitosan for controlled delivery of brassinosteroids with biological activity as agrochemicals. Carbohydrate Polymers 80, 915–921, doi:https://doi.org/10.1016/j.carbpol.2010.01.006 (2010).
87. Organization, W. H. *Pesticide Residues in Food, 1997: Report of the Joint Meeting of the FAO Panel of Experts on Pesticide Residues in Food and the Environment and the WHO Core Assessment Group on Pesticide Residues, Lyons, France 22 Sept.-1 Oct. 1997*. Vol. 145 (Food & Agriculture Org., 1998).
88. Khan, O. *et al.* Green synthesis and evaluation of calcium-based nanocomposites fertilizers: A way forward to sustainable agricultural. Journal of the Saudi Society of Agricultural Sciences, doi:https://doi.org/10.1016/j.jssas.2021.06.005 (2021).
89. Yadav, V. K. *et al.* The Processing of Calcium Rich Agricultural and Industrial Waste for Recovery of Calcium Carbonate and Calcium Oxide and Their Application for Environmental Cleanup: A Review. Applied Sciences 11, doi:10.3390/app11094212 (2021).
90. Vijai Anand, K. *et al.* Preparation and characterization of calcium oxide nanoparticles from marine molluscan shell waste as nutrient source for plant growth. Journal of Nanostructure in Chemistry, doi:10.1007/s40097-020-00376-4 (2021).
91. Anantharaman, A., Ramalakshmi, S. & George, M. Green synthesis of calcium oxide nanoparticles and its applications. Int. J. Eng. Res. Appl 6, 27–31 (2016).
92. Kolenčík, M. *et al.* Effect of Foliar Spray Application of Zinc Oxide Nanoparticles on Quantitative, Nutritional, and Physiological Parameters of Foxtail Millet (Setaria italica L.) under Field Conditions. Nanomaterials 9, 1559 (2019).
93. Yuvaraj, M. & Subramanian, K. S. Carbon sphere-zinc sulphate nanohybrids for smart delivery of zinc in rice (Oryza sativa L). Scientific Reports 11, 1–13 (2021).
94. Bala, R., Kalia, A. & Dhaliwal, S. S. Evaluation of Efficacy of ZnO Nanoparticles as Remedial Zinc Nanofertilizer for Rice. Journal of Soil Science and Plant Nutrition 19, 379–389, doi:10.1007/s42729-019-00040-z (2019).
95. Rossi, L., Fedenia, L. N., Sharifan, H., Ma, X. & Lombardini, L. Effects of foliar application of zinc sulfate and zinc nanoparticles in coffee (Coffea arabica L.) plants. Plant Physiology and Biochemistry 135, 160–166, doi:https://doi.org/10.1016/j.plaphy.2018.12.005 (2019).
96. Hasanpoor, M., Aliofkhazraei, M. & Delavari, H. Microwave-assisted Synthesis of Zinc Oxide Nanoparticles. Procedia Materials Science 11, 320–325, doi:https://doi.org/10.1016/j.mspro.2015.11.101 (2015).
97. Devi, R. S. & Gayathri, R. Green synthesis of zinc oxide nanoparticles by using Hibiscus rosa-sinensis. International Journal of Current Engineering and Technology 4, 2444–2446 (2014).

# Figures

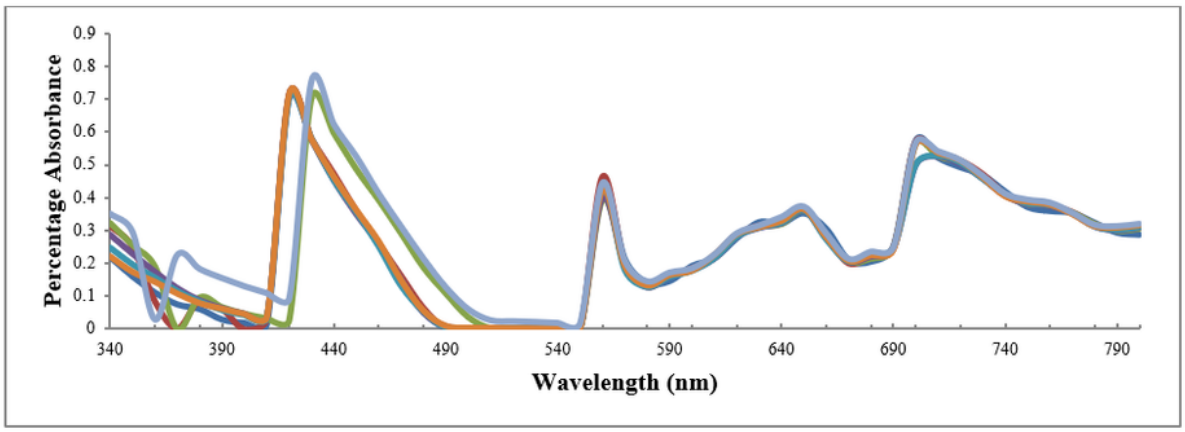


Ethephon

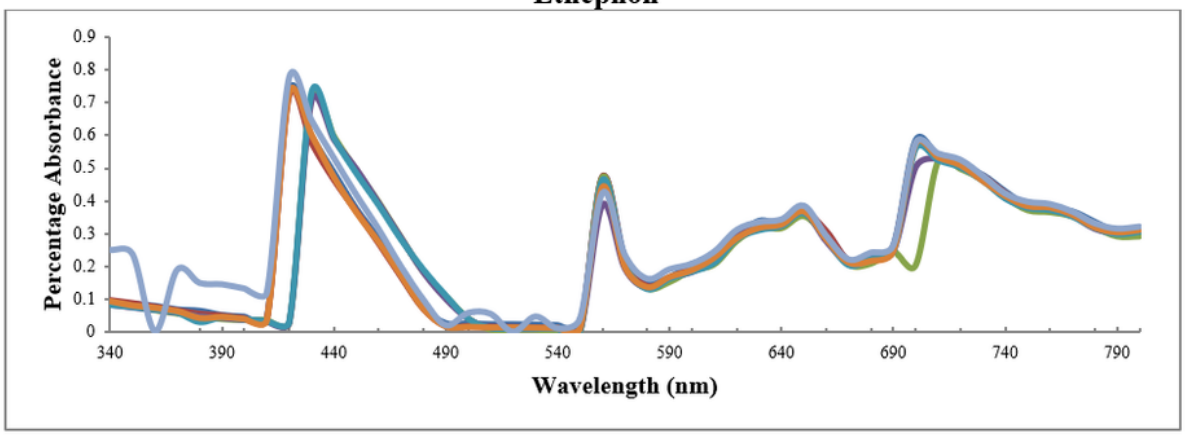


Ethephon-Si-NPs

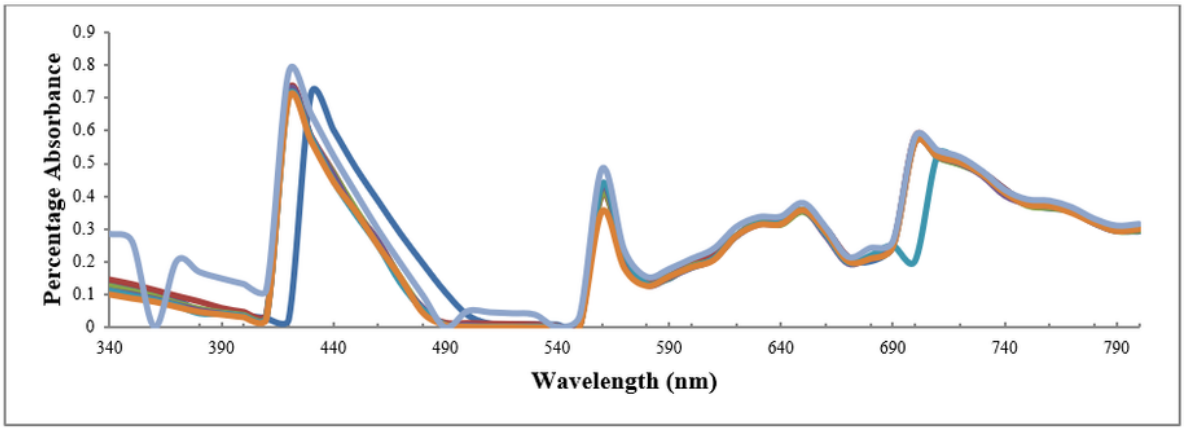


Ethephon-Zn-NPs

## Figure 1

Thermaldegradation profile of ethephon, ethephon-Si-NPs and ethephon-Zn-NPs

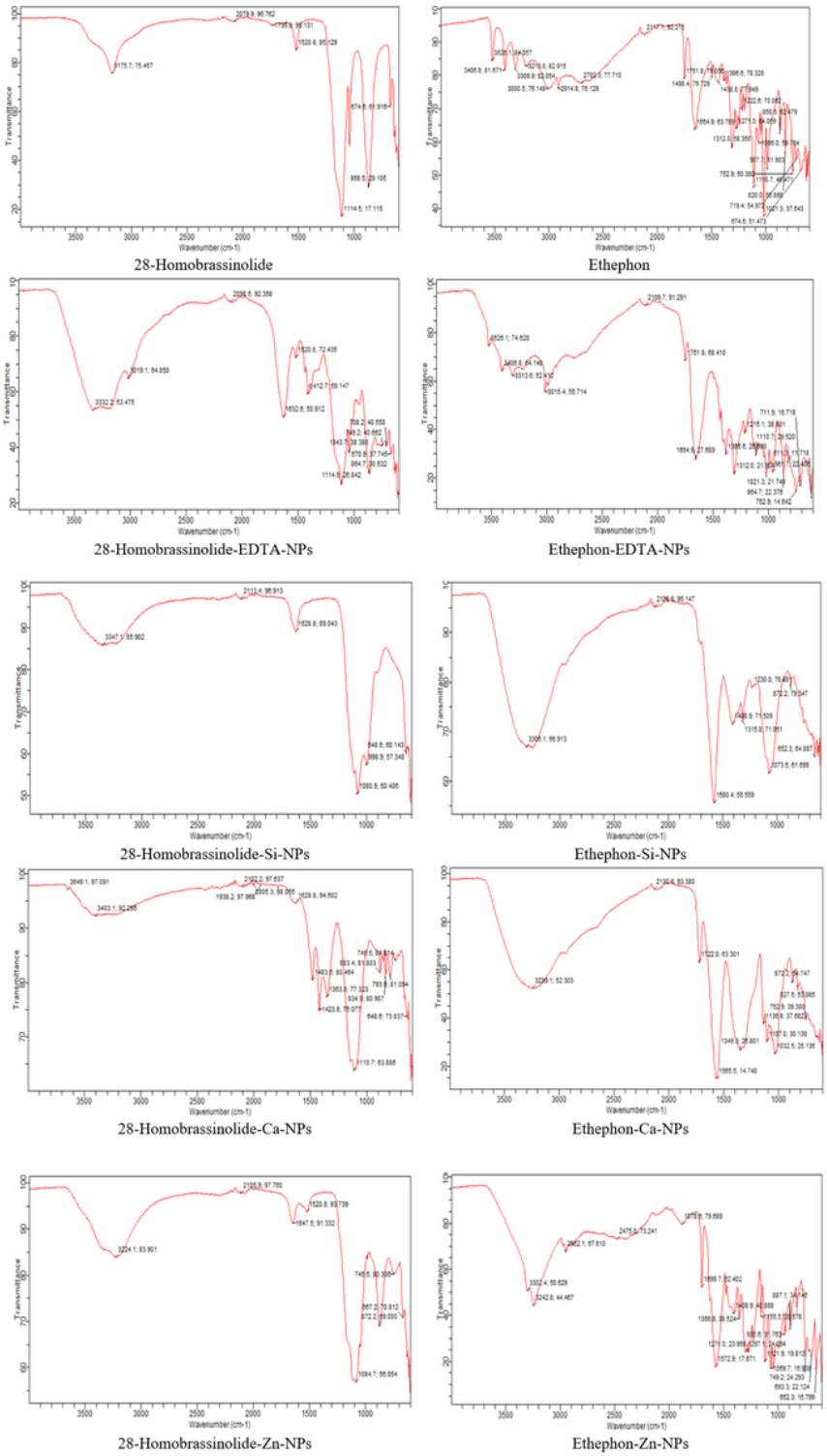


## Figure 2

Fourier transform infrared (FTIR) spectroscopic analysis

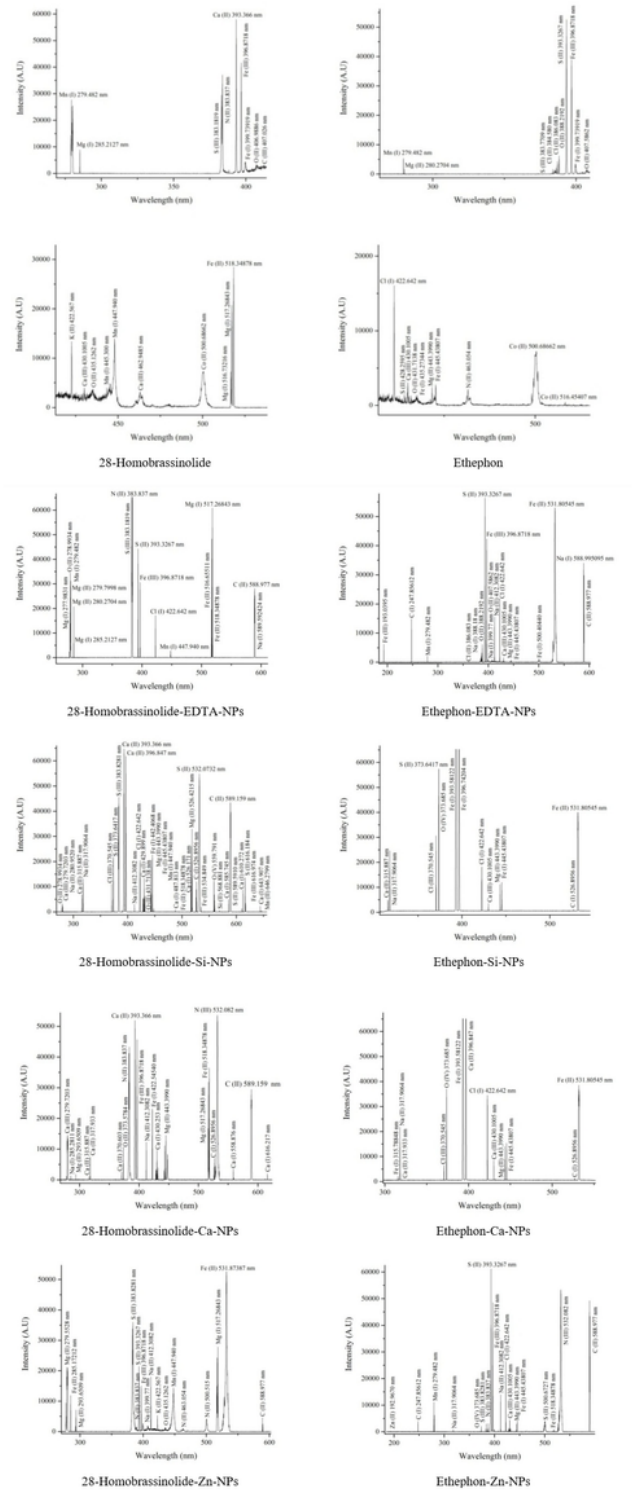


## Figure 3

Laser induced breakdown spectroscopic (LIBS) analysis

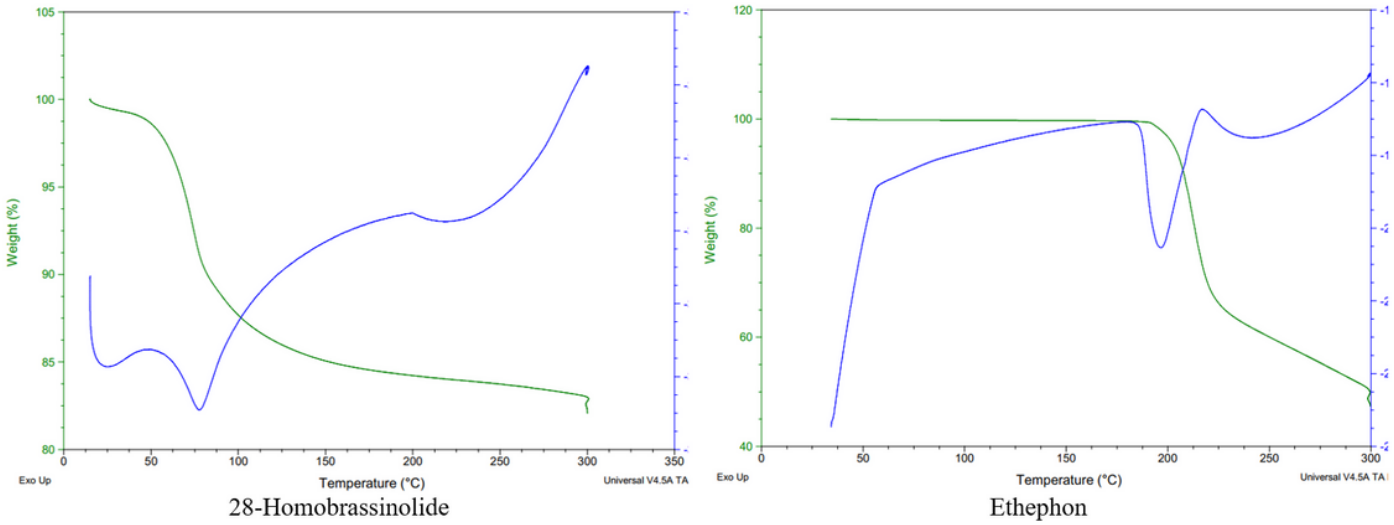


## Figure 4

Differential scanning colorimetry–thermogravimetric analysis (DSC-TGA)

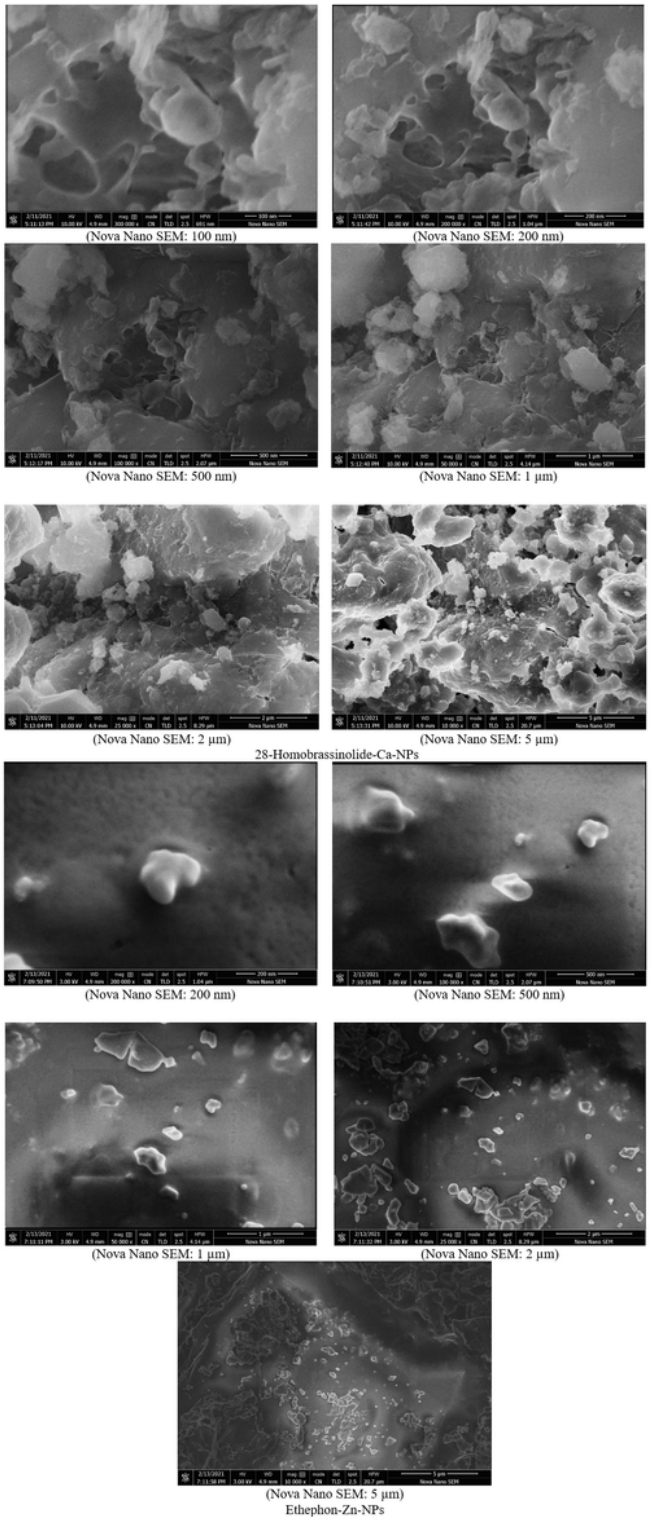


## Figure 5

Scanning electron microscopic (SEM) images